AGU PUBLICATIONS

JGR

Journal of Geophysical Research: Atmospheres

RESEARCH ARTICLE

10.1002/2015JD023742

Key Points:
- Coupled atmosphere-vegetation-aerosol model study of the last glacial maximum
- Two dust emissions schemes show similar agreement with paleodust data
- Dust radiative forcing varies between −0.4 and −1.2 W m^{-2} in the two schemes

Supporting Information:
- Texts S1–S4 and Figures S1–S7

Correspondence to:
P. O. Hopcroft,
peter.hopcroft@bristol.ac.uk

Citation:
Hopcroft, P. O., P. J. Valdes, S. Woodward, and M. M. Joshi (2015), Last glacial maximum radiative forcing from mineral dust aerosols in an Earth System model, *J. Geophys. Res. Atmos.*, *120*, 8186–8205, doi:10.1002/2015JD023742.

Received 1 JUN 2015
Accepted 28 JUL 2015
Accepted article online 30 JUL 2015
Published online 24 AUG 2015

©2015. The Authors.
This is an open access article under the terms of the Creative Commons Attribution License, which permits use, distribution and reproduction in any medium, provided the original work is properly cited.

Last glacial maximum radiative forcing from mineral dust aerosols in an Earth system model

Peter O. Hopcroft[1], Paul J. Valdes[1], Stephanie Woodward[2], and Manoj M. Joshi[3,4]

[1]Bristol Research Initiative for the Dynamic Global Environment, School of Geographical Sciences, University of Bristol, Bristol, UK, [2]Met Office Hadley Centre, Exeter, UK, [3]Ocean and Atmospheric Sciences, University of East Anglia, Norwich, UK, [4]Climatic Research Unit, University of East Anglia, Norwich, UK

Abstract The mineral dust cycle in preindustrial (PI) and Last Glacial Maximum (LGM) simulations with the Coupled Model Intercomparison Project Phase 5 model Hadley Centre Global Environment Model 2-Atmosphere (HadGEM2-A) is evaluated. The modeled global dust cycle is enhanced at the LGM, with larger emissions in the Southern Hemisphere, consistent with some previous studies. Two different dust uplift schemes within HadGEM2 both show a similar LGM/PI increase in total emissions (60% and 80%) and global loading (100% and 75%), but there is a factor of 3 difference in the top of the atmosphere net LGM-PI direct radiative forcing (−1.2 W m^{-2} and −0.4 W m^{-2}, respectively). This forcing is dominated by the short-wave effects in both schemes. Recent reconstructions of dust deposition fluxes suggest that the LGM increase is overestimated in the Southern Atlantic and underestimated over east Antarctica. The LGM dust deposition reconstructions do not strongly discern between these two dust schemes because deposition is dominated by larger (2–6 μm diameter) particles for which the two schemes show similar loading in both time periods. The model with larger radiative forcing shows a larger relative emissions increase of smaller particles. This is because of the size-dependent friction velocity emission threshold and different size distribution of the soil source particles compared with the second scheme. Size dependence of the threshold velocity is consistent with the theory of saltation, implying that the model with larger radiative forcing is more realistic. However, the large difference in radiative forcing between the two schemes highlights the size distribution at emission as a major uncertainty in predicting the climatic effects of dust cycle changes.

1. Introduction

Mineral dust aerosols are an important, natural component of the Earth system. They exert a direct influence on Earth's radiation balance by scattering and absorbing radiation in the atmosphere [*Tegen et al.*, 1996; *Haywood and Boucher*, 2000], potentially influencing regional meteorology [*Yoshioka et al.*, 2007]. Additionally, dust particles can act to modify the distribution and radiative properties of clouds [e.g., *Sassen et al.*, 2003; *Ansmann et al.*, 2008]. Dust is also thought to provide a source of nutrients to the ocean biological cycle [e.g., *Martin*, 1990] and tropical rainforests [e.g., *Koren et al.*, 2006; *Bristow et al.*, 2010]; thus, dust potentially influences atmospheric CO_2 through changes to the carbon cycle. Dust sources and sinks are also sensitive to climate and respond on long glacial-interglacial timescales [*Lambert et al.*, 2008] as well as over much shorter timescales in both past [e.g., *Wolff et al.*, 2010] and contemporary climates [*Prospero and Lamb*, 2003]. Dust is therefore intricately linked with many of the processes that regulate climate on a variety of spatial and temporal scales. However, our understanding of the magnitude of many of these feedbacks remains limited and models display a range of behaviors for modern-day climatic conditions [e.g., *Huneeus et al.*, 2011].

It is evident from ice core and other records that the dust cycle was more active during the Last Glacial Maximum (LGM: 24–18 kyr before present) than during the preindustrial (PI) era [*Kohfeld and Harrison*, 2001; *Lambert et al.*, 2008; *Maher et al.*, 2010]. Reconstructions of dust deposition rates from across the globe indicate increases by between 2 and 35 times, particularly over the poles. The LGM climate was globally around 4–6°C cooler than modern [e.g., *Braconnot et al.*, 2007] and was characterized by a much lower atmospheric level of CO_2 [*Petit et al.*, 1999] as well as major Northern Hemisphere ice sheets in North America and Europe [e.g., *Clark et al.*, 2009]. The colder and dryer climate and the reductions in global vegetation coverage are thought to be the prime drivers of this dust increase [*Harrison et al.*, 2001]. The inferred increase in atmospheric dust loading is thought to have caused additional cooling in the climate system [e.g., *Claquin et al.*, 2003; *Schneider von Deimling et al.*, 2006] through the direct radiative effect of dust aerosols. Climate modeling studies of the

LGM climate routinely neglect this dust forcing [*Braconnot et al.*, 2007], and this may introduce bias between modeled and reconstructed climates, or when climate sensitivity is estimated from LGM climate reconstructions [*Hargreaves et al.*, 2012].

A small number of studies have aimed to quantify the change in mineral dust loading at the LGM, not only to evaluate models of dust emissions and transport [*Andersen et al.*, 1998; *Mahowald et al.*, 1999; *Lunt and Valdes*, 2002; *Mahowald et al.*, 2006a] but also to quantify the LGM-PI radiative forcing [*Claquin et al.*, 2003; *Mahowald et al.*, 2006b; *Takemura et al.*, 2009; *Yue et al.*, 2011; *Albani et al.*, 2014]. The latter can help to clarify the relationship between temperature change and climate sensitivity at the LGM.

Though earlier studies did not take account of changes in vegetation distribution at the LGM [*Andersen et al.*, 1998], more recent modeling exercises made use of predictive vegetation model results in order to specify the vegetation effect on dust source regions. For example, *Mahowald et al.* [1999] employed the simulations of PI and LGM vegetation distributions from BIOME3. Global dust emissions were simulated to increase by a factor of 3, with much of this increase due to the simulated reduction in vegetation density. Other studies based on a similar methodology have found approximately similar increases in dust emissions at the LGM. For example, *Werner et al.* [2002], *Takemura et al.* [2009], *Yue et al.* [2011], and *Mahowald et al.* [2006a] all found an increase in dust emissions by a factor close to 2.4.

Claquin et al. [2003] were the first to incorporate these newer estimates of dust fluxes into a radiative transfer model. Using the dust loading simulated by *Mahowald et al.* [1999], they found that over the tropics the LGM-PI radiative forcing was of a similar magnitude to that resulting from the reduced greenhouse gas concentrations. *Mahowald et al.* [2006b] used the NCAR (National Center for Atmospheric Research) Community Climate System Model, version 3.0, to estimate the radiative forcing due to LGM dust compared with PI dust aerosols. The diagnosed radiative forcing in the model was between −0.5 and −1 W m^{-2}, in the middle range of the estimates of *Claquin et al.* [2003], but with a substantially smaller forcing over the tropics. *Takemura et al.* [2009] and *Yue et al.* [2011] calculated a direct radiative forcing of 0.1 W m^{-2} and −0.01 W m^{-2} at the tropopause and top of the atmosphere (TOA), respectively. More recently, *Albani et al.* [2014] present an improved version of the dust scheme used by *Mahowald et al.* [2006a] and simulate a smaller net LGM-PI radiative forcing of −0.1 W m^{-2}. Previous studies therefore mostly calculated a negative forcing from dust, but the range of values is large, spanning −2.0 to +0.1 W m^{-2}.

Here we use simulations with an atmosphere-vegetation-aerosol model (Hadley Centre Global Environment Model 2-Atmosphere (HadGEM2-A)) in order to explore the role of atmospheric dust at the Last Glacial Maximum. HadGEM2 has been used extensively as part of Coupled Model Intercomparison Project Phase 5 (CMIP5) [*Jones et al.*, 2011] and to examine decadal variability in the North Atlantic climate [*Booth et al.*, 2012]. With this model, we have the opportunity to assess the role of dust in a climatic state substantially different from modern. Our study is unique in that we utilize two different representations of dust uplift within the same climate model in order to explore the role of uplift parameterizations in the large-scale dust response under a changed climate. This follows a similar comparison for modern climate performed by *Ackerley et al.* [2012]. We perform a detailed comparison between the reconstructed and modeled dust deposition rates at the LGM in order to evaluate the model performance. Finally, we calculate the radiative forcing from dust and compare this with other major forcing and feedback factors operating during the LGM.

2. Methods

2.1. Model

In this study, we use the atmosphere, land surface, and aerosol components of the HadGEM2 model [*Collins et al.*, 2011; *HadGEM2 Development Team*, 2011] in atmosphere-only configuration which we here call HadGEM2-A (atmosphere only). The only difference in the atmosphere with the CMIP5 model HadGEM2-ES (Earth system) is that here we do not include the interactive tropospheric chemistry. HadGEM2 is a semi-Lagrangian, nonhydrostatic, fully compressible atmospheric general circulation model (GCM) [*Martin et al.*, 2006; *HadGEM2 Development Team*, 2011] used extensively in CMIP5 [*Jones et al.*, 2011]. In the atmosphere model, there are 38 unequally spaced levels in the vertical direction, with a horizontal resolution of 1.875° × 1.25° in longitude-latitude. HadGEM2 includes a comprehensive representation of seven aerosol species: mineral dust, sulfate, sea salt, biogenic emissions, biomass burning, and fossil fuel black carbon and organic carbon as described by *Bellouin et al.* [2007, 2011]. HadGEM2 makes use of the Top-Down Representation of Interactive Foliage and Flora Including Dynamics (TRIFFID) dynamic vegetation scheme

[*Cox et al.*, 2000; *Cox*, 2001] and an updated version of the Met Office Surface Energy Scheme land surface scheme [*Essery et al.*, 2003] which uses fractional tiling of nine land surface types, of which there are five plant functional types.

The emissions of mineral dust are calculated at each model time step and are dependent on the wind speed, soil moisture content, the vegetation fraction of a grid cell (as simulated by the TRIFFID model), the fractional content of each size division, and a preferential dust source multiplier field [*Woodward*, 2001; *Bellouin et al.*, 2007; *Woodward*, 2011]. The horizontal dust flux is computed in nine bins across a size range of 0.0316 to 1000.0 μm radius. From this, the vertical flux of particles smaller than 31.6 μm is calculated in six bins and emitted into the model atmosphere where dust is treated as six separate tracers. The horizontal flux is calculated according to the method of *Marticorena and Bergametti* [1995] using threshold friction velocities for each size particle from *Bagnold* [1941]. The effects of soil moisture are accounted for following *Fécan et al.* [1999].

The model simulates dry deposition by gravitational settling and turbulent mixing within the model boundary layer and wet deposition. Scavenging coefficients and radiative properties are derived from observations [*Balkanski et al.*, 2007; *Woodward*, 2011]. The radiative properties as a function of particle size are given in Table A1 of *Bellouin et al.* [2011]. For CMIP, the different HadGEM2 configurations (ES and A) have slightly different dust model parameters to account for the sensitivity of the emissions model to modeled or prescribed vegetation cover and differences in the wind field and soil moisture. In this study, we use the ES model dust parameters as used by *Bellouin et al.* [2011], because here we use dynamic rather than prescribed vegetation distributions.

Sea-salt aerosol numbers are also calculated interactively within HadGEM2-A as a function of near-surface wind speeds over open-ocean grid points [*Jones et al.*, 2001]. The remaining aerosol species are dependent on prescribed monthly emission fields which follow the preindustrial fields used for CMIP5 [*Jones et al.*, 2011]. All aerosols except biogenic secondary aerosols and sea-salt aerosols are transported by the atmospheric GCM at each time step within the model. In these simulations, the interactive atmospheric chemistry model United Kingdom Chemistry and Aerosols is not included and so the oxidizing capacity of the atmosphere with respect to sulfate remains at prescribed preindustrial levels.

All of the modeled aerosols influence long- and short-wave radiations and have an implicit semidirect effect on the climate. First and second indirect effects are also computed for all species except mineral dust and fossil fuel black carbon [*Bellouin et al.*, 2011]. Dust radiative effects are included in all simulations presented, except those in which the dust radiative forcing was calculated. These diagnostic simulations are described further below.

The preindustrial and LGM simulations with HadGEM2-A that constitute the main simulations analyzed here are described in detail by *Hopcroft and Valdes* [2014] with a focus on the dynamic vegetation results and comparison with paleoclimate data. In this study, it was found that to successfully simulate the LGM climate with HadGEM2, the leaf phenology model parameters required retuning as the parameters used in the CMIP5 version of HadGEM2-ES resulted in major deficiencies in the global simulation of LGM vegetation distribution. The model version used here is therefore the optimal tuned version of *Hopcroft and Valdes* [2014].

The boundary conditions basically follow the Paleoclimate Modelling Intercomparison Project 2 (PMIP2) protocol so that the preindustrial simulation is very similar to the CMIP5 HadGEM2-ES piControl simulation (though here we deactivate fossil fuel aerosols). The preindustrial simulation also includes a disturbance mask reconstructed for AD1860 which restricts the dynamic vegetation to grasses following the reconstructed distribution of crops or pasture [*Jones et al.*, 2011]. The LGM simulation differs from the PI in terms of the (i) insolation, which is modified for astronomic conditions of 21 kyr, (ii) concentrations of CO_2, CH_4, and N_2O which are reduced according to ice core data following the PMIP protocol *Braconnot et al.* [2007], and (iii) ice sheets and sea level, which are prescribed according to the ICE-5G reconstruction of 21 kyr [*Peltier*, 2004]. The agricultural disturbance mask is not used in the LGM simulations. In these atmosphere-only simulations, sea surface temperatures and sea ice distributions are prescribed from corresponding PI and LGM simulations with the coupled GCM Hadley Centre Coupled Model, version 3 [*Singarayer and Valdes*, 2010]. All simulations are 50 years long and follow an initial equilibrium phase in which the vegetation is updated using an implicit time step to reach near equilibrium. All PI and LGM simulations are initialized from the same respective initial conditions. Climatologies are based on the final 30 years of each simulation.

2.2. Alternative Dust Emission Scheme

In addition to the default version of HadGEM2 in which the aerosol model is called Coupled Large-Scale Aerosol Simulator for Studies in Climate (CLASSIC) [*Bellouin et al.*, 2011], we have modified HadGEM2 to incorporate the surface dust emission scheme (Dust Entrainment and Deposition (DEAD)) of *Zender et al.* [2003]. This follows the implementation in a prior version of the HadGEM2 by *Ackerley et al.* [2009, 2012]. While both schemes are based on *Marticorena and Bergametti* [1995] and *Fécan et al.* [1999], the implementation of the threshold friction velocity is different. The two schemes are described in detail in the supporting information.

A comparison of an older version of the dust model [based on *Woodward*, 2001] and the DEAD scheme is presented by *Ackerley et al.* [2012], showing a significant difference in the size profile of dust particles uplifted in the two schemes. The DEAD scheme showed a higher proportion of fine (<1μm radius) particles which is in better agreement with the Dust Outflow and Deposition to the Ocean measurements of *McConnell et al.* [2008] downstream of the Sahara considering the three smaller size divisions. The different size distribution of uplifted particles in the DEAD scheme makes it an interesting candidate for testing against large climatic changes such as the LGM. It is also important to note that neither of the model versions includes an explicit glaciogenic source of dust.

2.3. Radiative Forcing Calculations

In order to quantify the total direct effects arising from changes in the dust aerosol loading, we performed additional simulations wherein the radiation code of the model was used in a double-call formulation [see *Woodward*, 2001; *Bellouin et al.*, 2011]. At each radiation model time step, the radiation code is called twice. In the first call, the radiative fluxes are calculated as in the standard model configuration, and including dust aerosols. In the second call which is used to advance the model to the next time step, the radiative effects from dust are set to zero. The difference in the radiative fluxes between the two steps then gives the radiative forcing due to dust. These diagnostic simulations will display somewhat different climatologies compared to the default model runs, since the radiative effects of dust do not influence the evolution of the model state. There will also be a difference in the dust fields themselves, as dust-atmosphere feedbacks are not included.

The double-call calculation is similar to the method used to diagnose the standard cloud radiative forcing but suffers from the same issue identified by *Soden et al.* [2004]. In the case of clouds, a masking effect can occur without any actual change in the cloud distribution where there are significant changes in the surface albedo. This has also been noted for dust in the case of the LGM [*Claquin et al.*, 2003].

To avoid this problem in calculating cloud radiative forcing (RF), the partial radiative perturbation (PRP) method (or the approximate version: APRP [*Taylor et al.*, 2007]) is used. In APRP, the atmosphere is represented as a single column with multiple scattering and absorptions for short-wave (SW) radiation beams. The APRP uses the GCM output for radiative fluxes at the surface and TOA to derive monthly gridded values of scattering and absorption. With a few simple assumptions about the properties of the atmosphere, the APRP technique has been shown to reproduce the PRP diagnostics to within a few percent. We incorporate the SW dust radiative effect (for aerosol direct effects) calculated within the GCM using the double-call method into the simplified representation of the atmosphere's SW radiation budget used in the APRP method. We calculate the SW total atmospheric contribution to planetary albedo with and without the dust effects and use the difference to calculate the SW dust radiative effect. This accounts for major changes in surface albedo at the LGM which can otherwise show up in a standard dust radiative forcing calculation. This is detailed in the supporting information. For the long-wave (LW) radiative forcing, we use the difference between the two radiation calls within the GCM as there is likely to be less of an impact from surface changes on the LW dust radiative effect which is dominated by changes at low latitudes.

2.4. Paleodust Reconstruction Data

We compare model simulations with data from sites in the DIRTMAPv3 database [*Maher et al.*, 2010] for which size distribution information is estimated, as described by *Albani et al.* [2014]. In that work, the dust flux values at each site were corrected to remove the contribution from larger particles which were not modeled. This data set includes some additional terrestrial sources compared to the older DIRTMAPv2 data set but overall has less sites. To complement this, we include 50 new data points from the Southern Hemisphere from *Kohfeld et al.* [2013] which have been normalized using a constant flux proxy. In this, the amount of the radioactive decay product thorium at a particular site is predicted as a function of water depth and site age. Variations from this prediction are used as a proxy for nonsedimentary input (e.g., redistribution by ocean currents) to the ocean core site [e.g., *Chase et al.*, 2001]. The data from *Kohfeld et al.* [2013] are particularly useful because

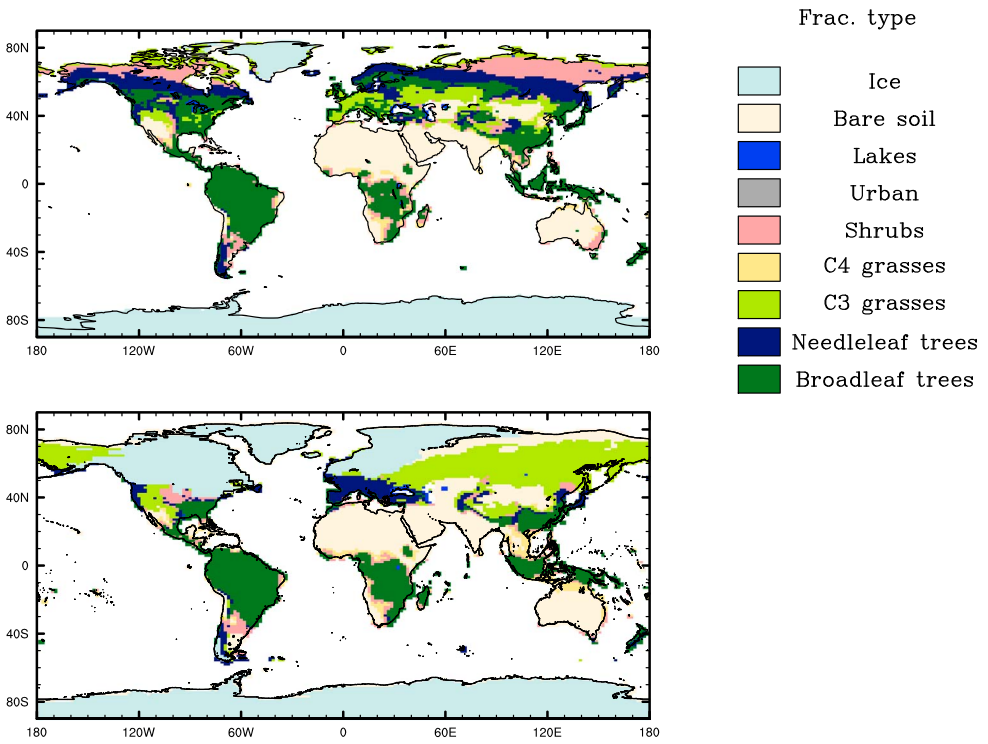

Figure 1. Dominant surface-type coverage in each grid cell in the (top) preindustrial and (bottom) LGM simulations.

they provide constraints on the change in dust deposition rates close to South America, where the sources of the majority of the LGM Southern Hemisphere dust are thought to have been located [*Delmonte et al.*, 2004; *Fischer et al.*, 2007]. Currently, there is no size distribution information for this latter data assemblage.

3. Results

3.1. Vegetation and Bare Soil Changes

Figures 1 and 2 show the dominant fractional land cover type and fractional bare soil coverage in the PI and LGM simulations. The dominant fractional coverage changes most markedly over Asia where much of the boreal forest in the PI is replaced with a combination of grasses, shrubs, and bare soil at the LGM. The global bare soil area expands from 45×10^6 to 63×10^6 km^2. This is mostly driven by vegetation reductions in Asia, Australia, and South America. The simulation of the dynamic vegetation is described in more detail in *Hopcroft and Valdes* [2014] where it is shown to be in reasonable agreement with paleovegetation reconstructions.

3.2. Dust Emissions

Figure 3 shows the annual mean dust emissions in the preindustrial and LGM simulations. The annual mean values are summarized in Figure 4 and Table 1. The dominant dust source regions in the preindustrial

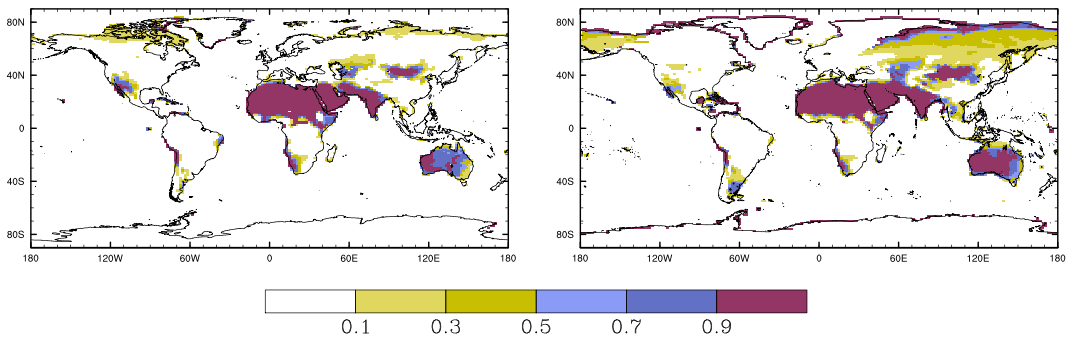

Figure 2. Bare soil fractional coverage in each grid cell in the (left) preindustrial and (right) LGM simulations.

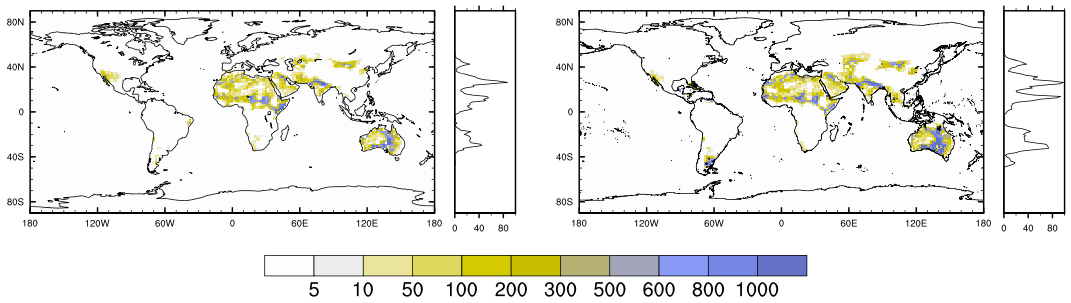

Figure 3. Annual mean dust emission distributions and zonal mean (kg m^{-2} s^{-1}) in HadGEM2-A simulations: preindustrial (left) and LGM (right).

simulation are the Sahara, Australia, and areas in Arabia and India (where the modeled modern-day monsoon is overly weak). At the LGM, all source regions intensify, with notable increases in the Patagonia area in South America and over parts of Australia. There are no significant extra dust-emitting regions north of around 50°N, probably because of a temperature limitation on emissions in the model and because emissions cannot occur when the ground is snow covered.

Comparison of the emission maps for the HadGEM2-A-DEAD simulations shows very similar spatial distribution as in the respective PI and LGM simulations shown in Figure 3. However, the total mass of dust emitted is approximately five times less and as shown in Figure 4 which shows the LGM/PI ratios for the emissions in each dust particle size division. The emissions are concentrated in size divisions 3–5 in DEAD, compared with 5–6 in CLASSIC. The two model versions do however show approximately similar mass of emissions in the central two divisions, numbers 2 and 4. Overall, therefore, the mode of the emissions in the DEAD scheme is at the radius of 1–3 μm, while in CLASSIC, emissions increase toward the largest size division.

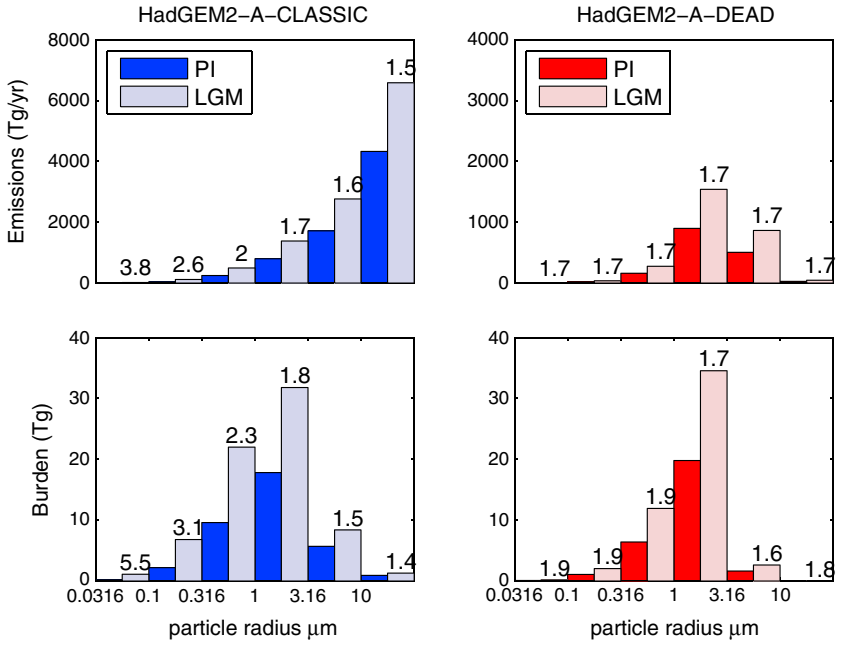

Figure 4. Dust emissions and loading by size division in the two schemes ((left) CLASSIC and (right) DEAD) for the PI and LGM model simulations. The LGM/PI ratios for each size division are overlain, showing larger relative changes for smaller particles in the CLASSIC scheme. Note that dust emissions diagnosed from the HadGEM2 model include all particles released from the surface, including those with a very short atmospheric lifetime. (In the code, these are redeposited by sedimentation in the same turbulent mixing subroutine that mixes the emissions into the atmosphere; hence, they never interact with the model atmosphere in any way.) As sedimentation on this timescale is significant for only the largest two bins, the size distribution of dust entering the model atmosphere is inevitably somewhat different from that shown here.

Table 1. Simulated Total Dust Emissions (Tg/yr), Atmospheric Burden (Tg), and Aerosol Optical Depth (AOD) at 0.55 μm Due To Dust and a Summary of Prior Work Including Two Models With Dust Schemes in CMIP5/PMIP3[a]

	Preindustrial			Last Glacial Maximum		
Model/Study	Emissions	Burden	AOD	Emissions	Burden	AOD
HadGEM2-A fixPIveg	3,563	-	0.029	4,367	-	0.043
HadGEM2-A	7,128	36	0.044	11,354	71	0.106
HadGEM2-A-DEAD	1,561	29	0.031	2,856	51	0.054
Werner et al. [2002]	1,060	8		2,383	23	
Claquin et al. [2003]	-	-	0.050	-	-	0.14
Mahowald et al. [2006a][b]	4,670	31	0.053	10,880	62	0.096
Takemura et al. [2009]	2,594	14	-	6,200	31	-
Yue et al. [2011]	1,966	28	0.032	4,579	67	0.077
Albani et al. [2014] (c4fn)	2,827	24	0.024	6,289	37	0.038
MIROC-ESM (CMIP5)	2,655	12	-	7,781	34	-
MRI-CGCM3[c](CMIP5)	2,119	14	-	2,919	19	-

[a]fixPIveg denotes HadGEM2-A simulations in which the vegetation distribution is static and prescribed in both the PI and LGM runs following satellite observations of *Loveland et al.* [2000].
[b]Excluding tuned glaciogenic sources.
[c]MRI-CGCM3 employs a modern vegetation distribution in both time periods.

The relative changes in emissions for the LGM are much larger in the smaller size divisions in the CLASSIC scheme, whereas they are constant across size divisions in the DEAD scheme. This is summarized in Figure 4. This enhanced sensitivity in CLASSIC can be understood in terms of the threshold friction velocity (u_{ti}^*) calculation, which is size dependent in CLASSIC but is assumed constant with particle size in this implementation of DEAD. The u_t^* values are larger for smaller particles. Since u_{ti}^* appears in the emission formulation, when $u_{ti}^* < u^*$, the emissions will scale with larger u_{ti}^*. The u_{ti}^* velocities are also subject to the same relative (i.e., %) change due to soil moisture, and so for the smaller size divisions which have higher dry threshold (u_{ti}^*) values, there are larger increases in u_{ti}^* at the LGM and hence larger absolute emissions change compared with the scheme with a single threshold friction velocity.

To confirm this hypothesis, we ran a modified pair of PI and LGM DEAD simulations in which the size-dependent threshold friction velocity formulation from CLASSIC is implemented. This had a large impact on the dust aerosol optical depth (AOD) at 0.55 μm, and the globally averaged LGM/PI ratio increased from 1.7 in DEAD to 2.5 (0.05 to 0.12 in the PI and LGM, respectively) in the modified version. This is very close to the ratio of 2.4 in CLASSIC. We therefore conclude that the size-dependent threshold friction velocity is very important for the radiative properties of dust loading in current schemes, a point we return to.

The monthly data for bare soil fraction and dust emissions averaged across China and Patagonia for the preindustrial and LGM simulations with the CLASSIC aerosols scheme are shown in Figure S1 of the supporting information. These areas are chosen because they have been previously identified as the most likely source regions for enhanced LGM dust deposition in Greenland and Antarctica, respectively [*Svensson et al.*, 2000; *Delmonte et al.*, 2004]. There is monthly variation in both the bare soil area and the dust emissions. However, the lack of a strong correlation between these two variables emphasizes the role of other seasonally varying parameters, particularly soil moisture and wind speed, which control the seasonal variability in the dust emissions.

3.3. Dust Deposition

Dust depositional change has been hypothesized as an important control of the ocean carbon cycle. Elevated dust input to the Southern Ocean could have fertilized ocean biology there, causing uptake of atmospheric CO_2 during the LGM [*Martin*, 1990], though process-based modeling suggests an upper limit to this effect of 30 ppmv [*Bopp et al.*, 2003] and other nondepositional sources of iron could be important [*Raiswell et al.*, 2007]. The total dust depositional change over the Southern Ocean (up to 40°S) is 58 Tg/yr to 212 Tg/yr in CLASSIC and 35 Tg/yr to 182 Tg/yr in DEAD. In this case, the relative changes are 3.7X and 5.2X, respectively, highlighting the larger relative changes in the DEAD scheme. Dust deposition is also thought to be important for Amazon rainforest as it is thought to constitute an important source of nutrients for ecosystems there [e.g.,

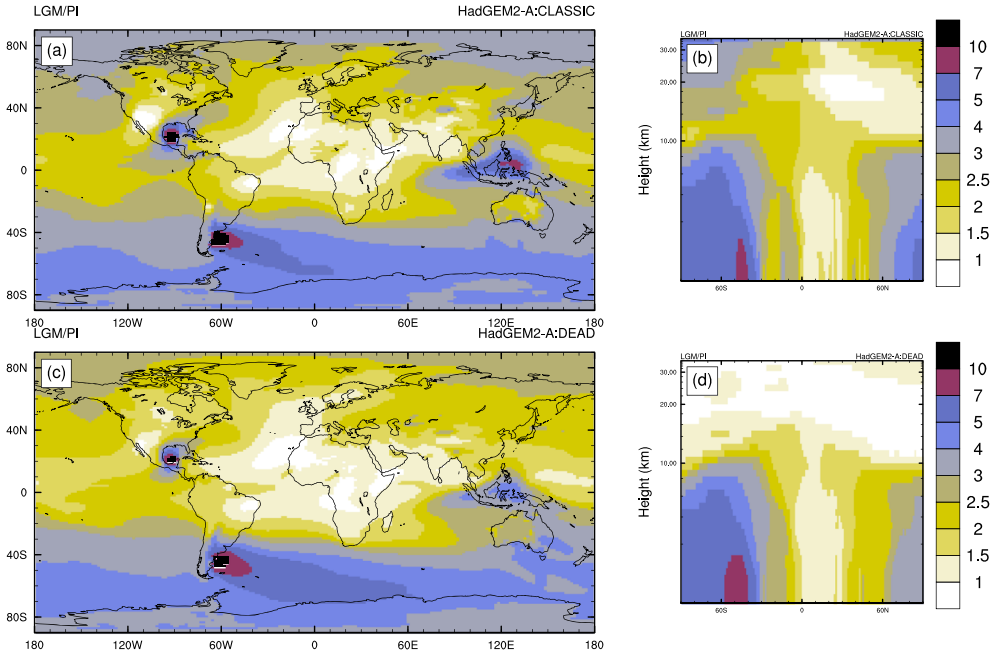

Figure 5. LGM/PI ratio of total column and zonally averaged latitude-height distribution of atmospheric dust loading (a and b) in HadGEM2-A CLASSIC and (c and d) in the DEAD scheme.

Koren et al., 2006; *Bristow et al.*, 2010]. In these simulations, the dust deposition over the Amazon (30°S–10°N and 80°W–30°W) increases from 57 Tg/yr to 71 Tg/yr in the CLASSIC formulation and from 28 Tg/yr in the preindustrial to 54T g/yr in the DEAD scheme. These are increases by factors of 36% and 92% for CLASSIC and DEAD, respectively. Thus, the relative change in the rate of dust deposition at the LGM is again much larger in the DEAD scheme.

3.4. Dust Loading

The simulated dust loading in each simulation (except the fixed PI vegetation runs for which appropriate output fields have not been saved) is shown in Figure 4 and Table 1. It is important to examine the simulated loading as, due to the structure of the model code, a small percentage of the emissions in bins 5 and 6 is resettled after emission within the same time step in HadGEM2 and has no impact on the radiation balance. The loading is reasonably consistent between the CLASSIC and DEAD simulations with values of 36 Tg and 29 Tg, respectively, in the preindustrial, increasing to 71 Tg and 51 Tg, respectively, in the LGM simulations. Comparison with prior work (summarized in Table 1) shows a large range in value for both time periods. The CLASSIC preindustrial value is higher than other work examined here, but the LGM value is similar to values simulated by *Yue et al.* [2011]. The interesting feature is that total column loading does not correlate well with total emitted flux, and this is because the larger and heavier particles have a shorter lifetime and so contribute less to the overall burden. The emissions in each bin (Figure 4) show that the heaviest bin dominates emissions in CLASSIC, while dust in size bin 4 dominates the loading in CLASSIC and DEAD for both the PI and LGM. The relative increase in burden in the first three bins (i.e., radii $< 1.0\mu m$) is much larger for CLASSIC compared to DEAD when considering the LGM relative to the PI, as shown by the LGM/PI loading ratios for each division, which are summarized in Figure 4.

Figure 5 shows the LGM/PI ratio of atmospheric dust loading both for the total column loading and for the zonally averaged latitude-height cross section. The relative changes in CLASSIC compared to DEAD are larger, especially in the high northern latitudes and above around 20 km height (Figures 5b and 5d). The larger changes in these regions in CLASSIC are predominantly driven by dust size divisions 1 and 2 (radii = 0.01–0.316μm), and this is supported by the larger relative changes (LGM/PI) in both emissions and loading in these smaller divisions in CLASSIC as shown in Figure (4). This is related ultimately to differences in the emissions schemes as noted in section 3.2.

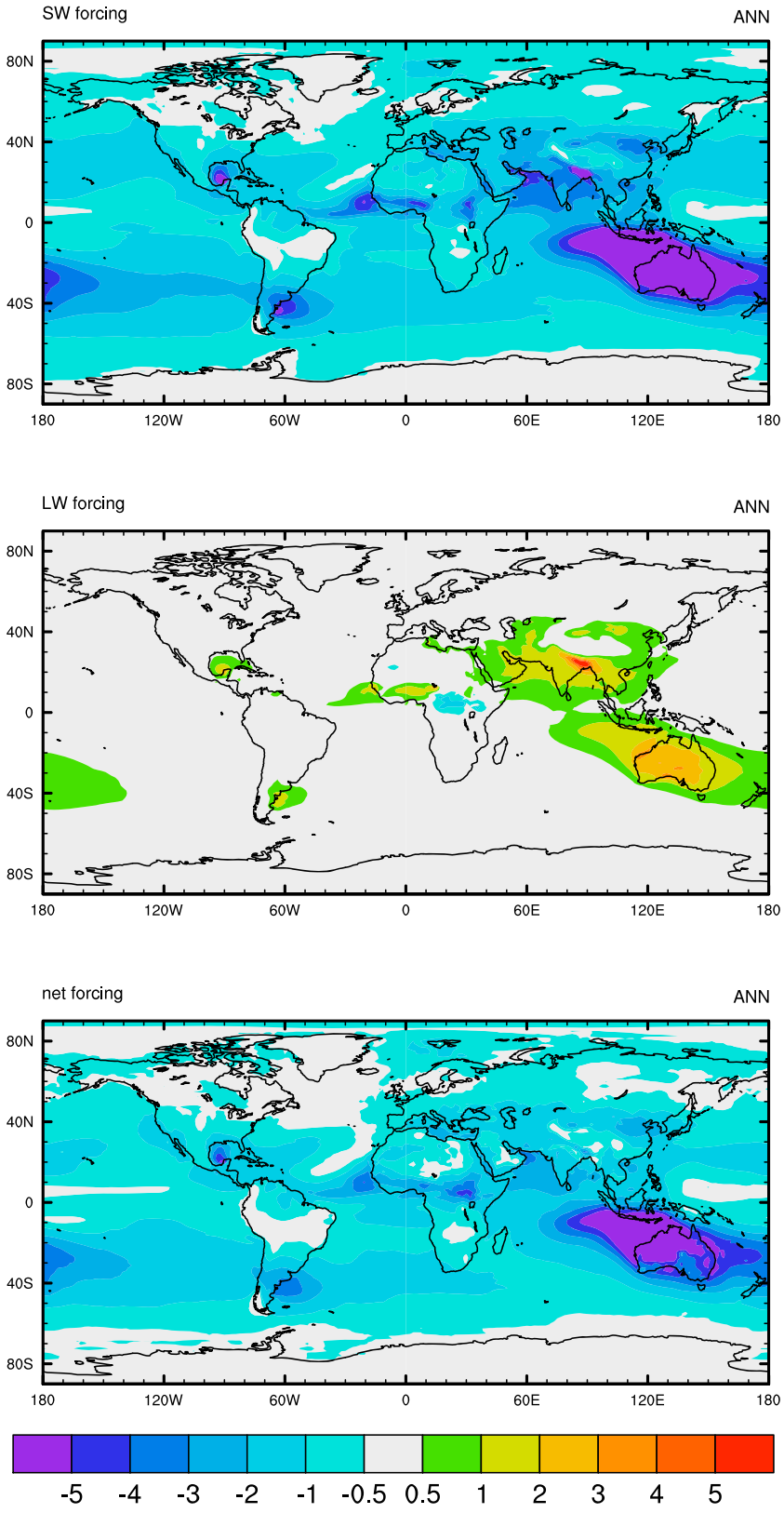

Figure 6. Radiative forcing for the aerosol direct effect (W m^{-2}) change LGM-PI for SW, LW, and net at the TOA in HadGEM2-A CLASSIC.

Table 2. Simulated Radiative Forcing at the TOA for LGM-PI[a]

Simulation	SW	LW	Net
HadGEM2-A fixPIveg	−0.56 (−0.50)	0.14	−0.42 (−0.36)
HadGEM2-A	−1.59 (−1.51)	0.41	−1.20 (−1.10)
HadGEM2-A-DEAD	−0.68 (−0.63)	0.32	−0.37 (−0.32)
Claquin et al. [2003][b]	-	-	−2.0
Mahowald et al. [2006a]	-	-	−0.53
Takemura et al. [2009]	−0.14	0.13	−0.01
Yue et al. [2011]	−0.58	0.68	0.1
Albani et al. [2014] (c4fn)	−0.17	0.08	−0.09

[a]SW forcing values are calculated using the extended APRP analysis. SW forcing values in brackets are calculated as in prior work which is summarized in the lower half of the table.
[b]Range of −2.0 to +0.2, depending on dust properties.

3.5. Dust Direct Radiative Forcing

Figure 6 shows the SW, LW, and net LGM-PI radiative forcing for the aerosol direct effect in the model. Here the LW forcing is calculated directly from the double-call radiation simulations, while the SW forcing is derived from the equivalent SW outputs using the APRP method as outlined in section 2 and the supporting information. The globally averaged values are summarized in Table 2. The total net changes vary between −0.37 and −1.20 W m^{-2} which is within the range estimated by other models. The results also highlight the importance of vegetation change. If the vegetation is held at the preindustrial distribution, the LGM-PI radiative forcing is reduced by around 50%. The globally averaged SW direct forcing of dust is negative at both the TOA and surface, while the LW forcing is positive, offsetting to some extent the SW effect. The largest radiative forcing changes are close to the Southern Hemisphere dust sources, particularly from Australia and from South America where the dust source is weak in the preindustrial simulation. The spatial patterns in radiative forcing are broadly similar to *Claquin et al.* [2003].

The major change between the direct calculation of the dust RF and that derived by APRP is the disappearance of areas of positive SW dust RF (see supporting information Figure S3) over the LGM ice sheet areas and a reduction in the RF over Asia where there is also an increase in surface albedo due to reduction in forest coverage and an increase in snow cover. This change increases the globally averaged SW dust forcing LGM-PI anomaly by 7% in both the standard and DEAD results, as shown in Table 2.

For comparison in Figure 7, the equivalent distributions are shown for the DEAD emission scheme simulations. The globally averaged SW forcing is now smaller at only −0.68 W m^{-2} compared to −1.59 W m^{-2} in the CLASSIC model formulation. The LW forcing in CLASSIC is larger though by 30% so that the net forcing in the DEAD simulation is 3.2 times smaller than in the CLASSIC simulations. The distributions of the dust radiative forcing are similar in the two schemes, suggesting that it is the particle size distribution of the uplifted dust rather than any difference in the spatial or temporal emission patterns that is the key to the differences between the CLASSIC and DEAD dust anomalies. This is confirmed by analysis of the dust loading in the two schemes, which shows larger changes in emissions and loading in the two smallest size divisions in the CLASSIC scheme (Figure 4). Additionally, the vertical distribution of loading (the total is shown in Figure 5) shows larger changes aloft in the CLASSIC scheme for the two smallest particle radii (not shown).

3.6. Comparison With Observed Deposition Rates

Figure 8 shows a comparison between the observational database and the model simulations for both the CLASSIC and DEAD scheme model simulations for the PI and LGM. This analysis shows very similar depositional values between the two models in both time periods, despite a much reduced total mass of emitted dust in the DEAD version. The modeled deposition by size bin is included in the supporting information, and this demonstrates that much of the longer-range depositional flux is dominated by size division 4 (radius 1–3.16 μm), for which emissions and burden in the two models (CLASSIC and DEAD) are comparable (see Figure 4).

Overall, the CLASSIC model performs relatively well at the ice core sites in Greenland but overestimates fluxes over Antarctica. The agreement with the new Southern Hemisphere data of *Kohfeld et al.* [2013] for the PI and

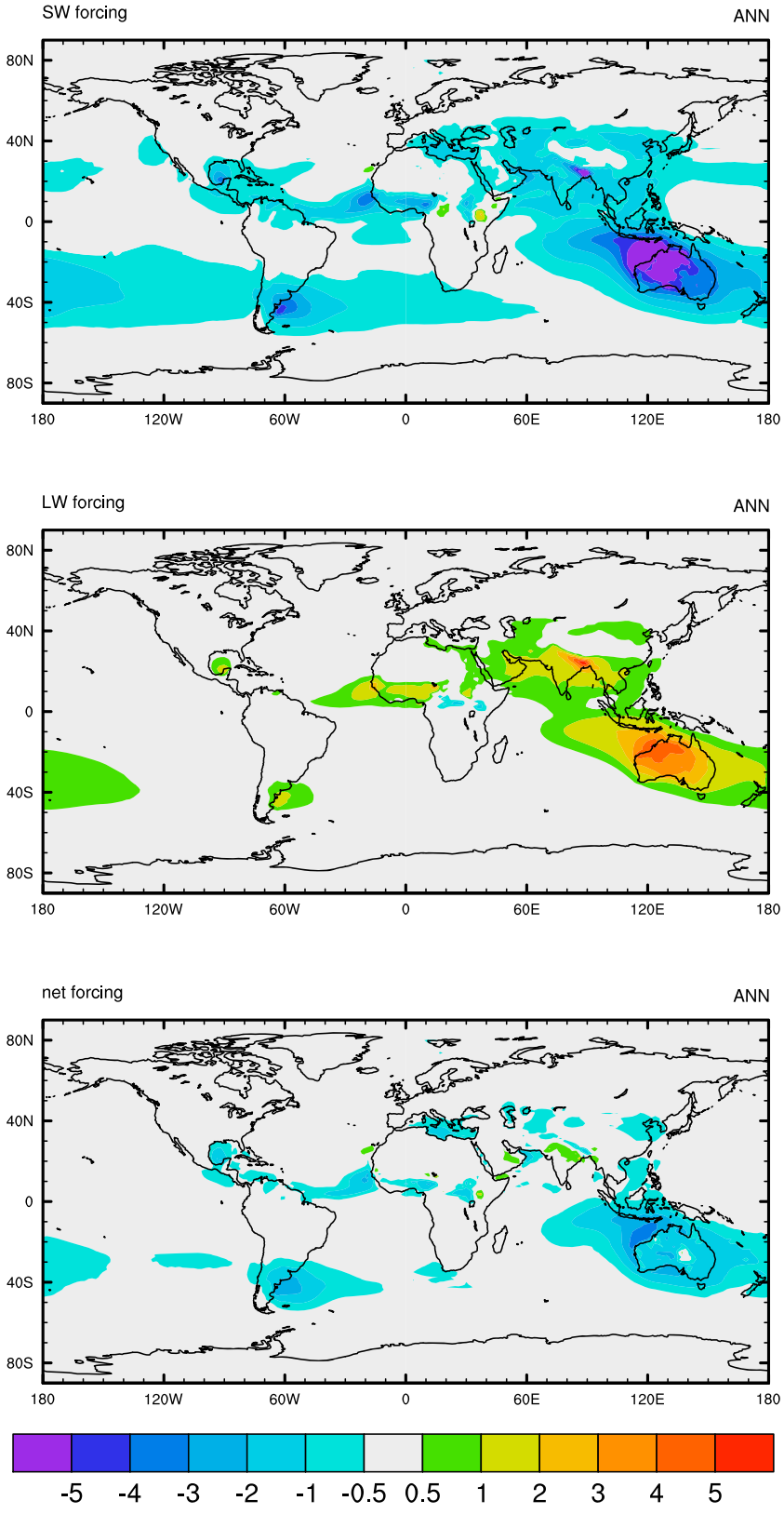

Figure 7. As in Figure 6 but for HadGEM2-A-DEAD.

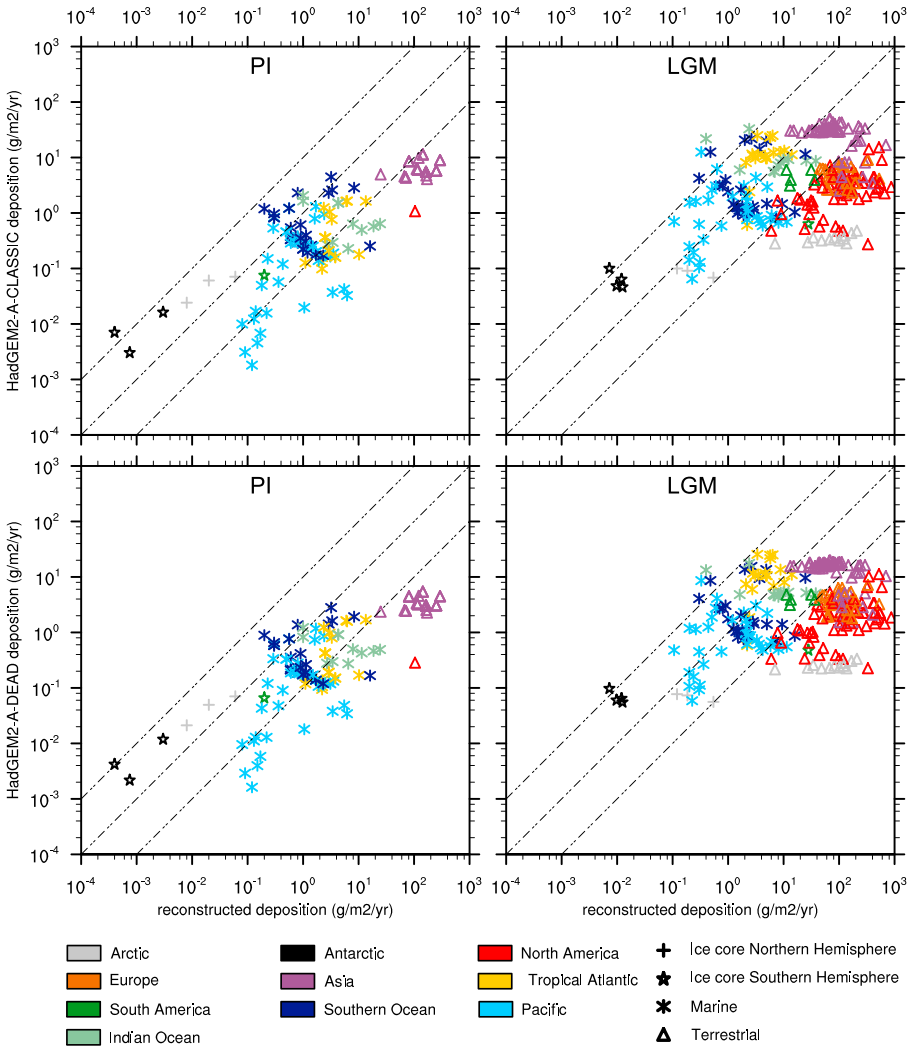

Figure 8. Scatter plot of modeled and observed dust deposition fluxes (g m^{-2} yr^{-1}) for the (top) CLASSIC and (bottom) DEAD scheme HadGEM2-A simulations of the (left) preindustrial and (right) LGM. Reconstructions are based on DIRTMAPv3 as compiled by *Albani et al.* [2014] and Southern Ocean data presented by *Kohfeld et al.* [2013]; the former assessed the fraction of reconstruction dust deposition in the particle range <10 μm relevant for model data comparison.

LGM is relatively good. In the preindustrial, the largest discrepancies are for terrestrial sites in North America and some of the Pacific sites.

At the LGM, the marine data are well captured by the models, but the estimates from the terrestrial sites are generally significantly underestimated by both models, particularly for Arctic, North America, and to a lesser extent Europe. Other terrestrial sites are relatively well reproduced in the model, for example, in South America and Asia.

Part of the underestimate of the terrestrial sites at the LGM could be caused by a missing glaciogenic source. *Mahowald et al.* [2006a] tuned a glaciogenic source to give a good fit to the reconstruction data and suggested that this (highly uncertain) source could provide missing sources to explain high deposition rates inferred for some regions at the LGM, particularly continental Asia and Greenland.

In Figure 9, we compare the ratio LGM/PI of dust deposition rates in the model with the DIRTMAP database. Overall changes in the tropics and parts of the Southern Ocean are reasonably well matched by the model, especially the increased depositional flux southeast of Patagonia and the moderate changes downwind of the Sahara over the equatorial Atlantic. Significant increased fluxes over Asia are not matched in the model.

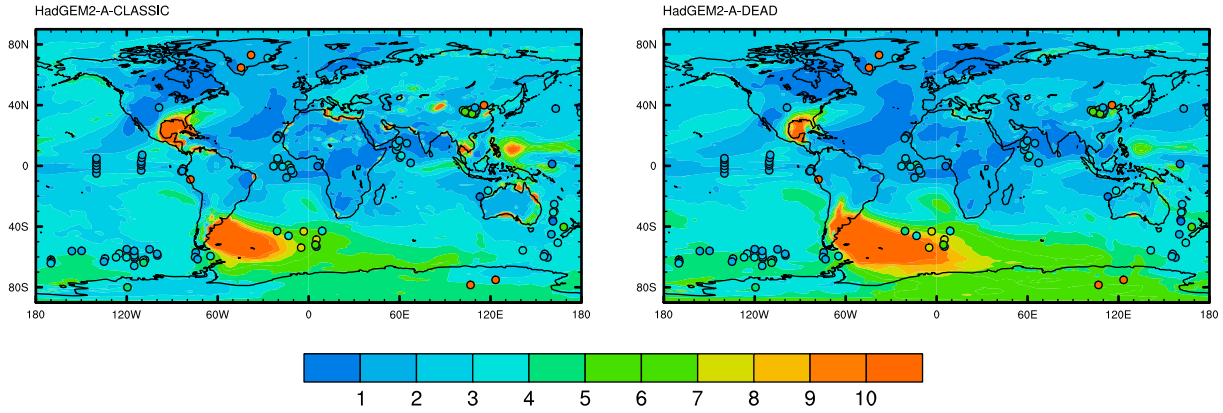

Figure 9. Comparison of the dust deposition ratio LGM/PI for HadGEM2-A model (left) CLASSIC version and (right) the DEAD dust scheme implemented with the DIRTMAPv3 data from *Albani et al.* [2014] and Southern Ocean deposition reconstructions from *Kohfeld et al.* [2013] (filled circles).

Regarding the ice core deposition changes, the DEAD model version is closer to the Antarctic ice core-derived flux increase of around 20 times [e.g., *Fischer et al.*, 2007; *Lambert et al.*, 2008]. However, this seems to be at the expense of predicting too high a depositional increase over the Southern Ocean downwind of the modeled LGM South American dust source (Figure 9). In the CLASSIC formulation, the model conversely shows a better match over the Southern Ocean while underestimating the flux change over the Antarctic continent. This is also corroborated by comparison with a new record from *Martinez-Garcia et al.* [2011] from ODP site 1090 (located at 43°S, 54°E) which is highlighted in Table 3. The ice core-inferred LGM/PI dust flux increase of up to 67 times over Greenland [*Fischer et al.*, 2007; *Maher et al.*, 2010] is not replicated by the either set of model simulations. This suggests that extra LGM high-latitude Northern Hemisphere source regions are required [for example, from glaciogenic sources: *Mahowald et al.*, 2006a] or that the parameterizations of source region and source material availability are undersensitive to cold climatic conditions.

3.7. Dust Size Distribution and Dust Concentration Observations

As the size distribution is important for assessment of the radiative effects of dust, we here compare the distribution of the deposition flux from the model schemes with ice core observations for both the PI and LGM time periods. Table 4 compares the percentage of measured and simulated dust in the range of the two smallest size divisions in the model (particle radii 0.0361 – 0.361 μm). The observational data are the same as compiled by *Albani et al.* [2014] but here recalculated for the HadGEM2 dust division sizes. This comparison shows that the CLASSIC scheme results are in better agreement with the observations for the preindustrial. The CLASSIC values are closer to the observations than the DEAD scheme at all sites except for Muztagata and Dasuopu, for which the two model schemes give very similar percentages. Crucially, at the very high latitudes in either pole, where long-range transport of the finer particles is important, the CLASSIC scheme simulates 6.1% and

Table 3. Simulated Dust Deposition Rates (Tg/yr) With Percentage Wet Deposition in Brackets and Deposition Ratios (LGM/PI) for Greenland, Two Antarctic Ice Core Sites, and an Example Southern Ocean Site[a]

	Deposition (Tg/yr)		Deposition Ratio LGM/PI			
Model/Data Set	PI	LGM	Greenland	EDC[c]	Byrd[d]	ODP[e]
HadGEM2-A fixPIveg	3560 (17%)	4353 (18%)	0.9	2.7	1.7	3.3
HadGEM2-A	7121 (18%)	11347 (20%)	1.5	4.2	2.9	5.1
HadGEM2-A-DEAD	1606 (59%)	2755 (59%)	1.3	5.7	3.6	6.3
Reconstructed[b]	-		15 – 20	10 – 15	1.5 – 4	5

[a]Site LGM/PI model deposition ratios in the rightmost three columns are summed over bins 2 – 5 for compatibility with the range of particle sizes in ice core measurements [e.g., *Albani et al.*, 2012], but these ratios are very similar when summed across all six bins.

[b]Data are Greenland: *Fischer et al.* [2007], EDC: *Albani et al.* [2012], Byrd: *Kohfeld and Harrison* [2001], and ODP1090: *Martinez-Garcia et al.* [2011].

[c]EPICA Dome C ice core site.

[d]Byrd ice core site.

[e]Southern Ocean site ODP1090: 43°S, 54°E.

Table 4. Percentage of Total Dust Deposition in the First Two Model Bins (Radii = 0.0361–0.361μm) in Observations and the HadGEM2-A Simulations With the CLASSIC and DEAD Dust Schemes

	Latitude	Longitude	Preindustrial			Last Glacial Maximum		
Study	(°N)	(°E)	Observations	CLASSIC	DEAD	Observations	CLASSIC	DEAD
Steffensen [1997][a]	75	−38	6.9	7.1	3.8	2.0	7.4	2.6
Wu et al. [2009]: Dunde	39	96	0.02	1.1	1.4	-	0.6	0.9
Wu et al. [2009]: Muztagata (7010)	38	75	0.5	3.8	2.4	-	4.3	2.1
Wu et al. [2009]: Dasuopu	28	85	0.004	2.4	1.7	-	1.6	1.0
McConnell et al. [2007]	−64	−58	14.9	11.3	5.2	-	11.7	3.9
Delmonte et al. [2002, 2004]	−75	123	6.1	4.1	1.4	1.5	3.6	0.8

[a]Holocene (1) and mean LGM (1–4) values.

4.1%, for Greenland and East Antarctica, respectively, compared with 6.9% and 6.1% in the observations. The DEAD scheme values are generally too low, with values at these two locations of 3.8% and 1.4%, respectively.

For the LGM, for which observations are only available from Greenland and Antarctic, the CLASSIC scheme simulates an increase in the finer particle percentage at Greenland and a small decrease in Antarctica, while the DEAD scheme is more realistic and correctly predicts a reduction in the fine-particle percentage at both poles. This comparison of the LGM to PI change is likely to be complicated by the underestimation of the total LGM dust deposition increase in both dust schemes, especially over Greenland.

The mass size distribution of dust emissions of the two schemes can be compared by calculating the clay fraction of *Kok* [2011] (defined as the percentage of particles smaller than 2 μm diameter in the size range up to 20 μm diameter, that is, the ratio of particles in HadGEM2 size bins 1–3 versus bins 1–5). This also allows comparison with the values from a number of other dust schemes analyzed by *Kok* [2011]. For the preindustrial simulations, the area-weighted average clay fraction is 4.8% and 11.5% for CLASSIC and DEAD, respectively. The CLASSIC value is therefore in excellent agreement with the empirically based formulation of *Kok* [2011] which predicts a clay fraction of 4.4 ± 1.0% and which shows good agreement with observed volume size distributions of dust emissions. The DEAD value is closer to other models analyzed by *Kok* [2011] for which the clay fraction value varied from around 9% to just over 35%. The good agreement of the size distribution formulation of *Kok* [2011] with the CLASSIC emissions implies that the size distribution of emissions in CLASSIC is more realistic than that predicted in this implementation of the DEAD scheme.

Some ambiguity is introduced in the above comparison because as noted already for HadGEM2 a proportion of the modeled emissions in the two larger size divisions are redeposited to the surface within a time step and so have no interaction with the atmospheric model. This effect is not directly quantifiable with the current code structure, except when a simulation is initialized with zero atmospheric dust loading. Doing so gives a global average value of around 30% for size bin 5. Reducing emissions by this amount in bin 5 leads to clay fraction values of 5.9% and 12.7% in CLASSIC and DEAD, respectively.

A comparison of the size distribution of near-surface concentrations in the Sahara region of the model shows that the two schemes are closer to each other than to observations [e.g., from *Ryder et al.*, 2013]. This is despite a significant difference at emission (shown in Figure 4 for the global average, but the relative values are similar in the Sahara region). Sedimentation of the larger particles in the model is significant, and the differences between the schemes at emissions become less significant in either the loading or depositional fluxes.

A comparison of the model outputs with modern observed dust concentrations from around the globe is presented in Figure S2 of the supporting information. Although this comparison is hindered by the fact that modern and preindustrial emissions are undoubtedly different, the comparison shows similar levels of agreement of the two model schemes.

3.8. Comparison With Other Forcing Factors

The forcing due to ice sheets and reduced greenhouse gases is known to constitute the major influences on the LGM climate as the astronomical term for 21 kyr is negligible and can be ignored. The combined greenhouse gas (GHG) term has been calculated by *Yoshimori et al.* [2009] as −2.85 W m^{-2}, though inter-model variability in this term is estimated as 0.4–0.6 W m^{-2}. *Braconnot et al.* [2012] derived values from six PMIP2 models for the instantaneous forcing due to the ice sheets and from feedbacks associated with

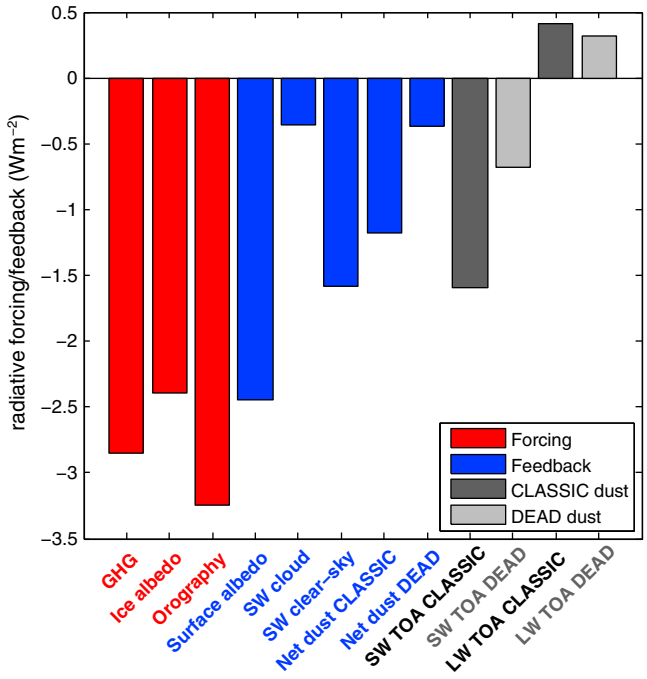

Figure 10. Globally averaged radiative forcing factors (red), feedbacks (blue), and dust feedback components (grey) in W m^{-2}. Forcings: approximate greenhouse gas forcing from *Yoshimori et al.* [2009], ice sheet albedo, and the Planck orographic forcing. Feedbacks: APRP-diagnosed surface albedo change, SW cloud radiative effects, SW clear sky (excluding dust), and mineral dust. The net dust radiative forcing is further broken down into SW and LW components in the grey bars. The dust radiative forcing for both the CLASSIC and DEAD emission scheme simulations is shown for comparison. See text for full description.

surface albedo and changes in clouds and other (nondust) atmospheric constituents. Here we perform a similar analysis using the APRP method [*Taylor et al.*, 2007] and include the LGM-PI dust direct radiative forcing for comparison. The Planck LW orographic forcing (i.e., the change in emitted surface LW radiation caused solely by altitude changes) is calculated using a uniform lapse rate of 6.5 K km^{-1}, following *Braconnot et al.* [2012].

This analysis is summarized in Figure 10. The global SW surface albedo feedback from snow and sea ice but not prescribed ice sheets (−2.5 W m^{-2}) is comparable to the surface albedo forcing from LGM ice sheets only (−2.4 W m^{-2}), while the global orographic term is larger at −3.2 W m^{-2}. The SW cloud feedback which is an important determinant of climate sensitivity is weakly negative, though with significant regional variations. There is a substantial contribution in the model from changes in clear-sky short-wave feedback of −1.1 W m^{-2}. The only other aerosol to change significantly is sea-salt aerosol, but this shows a reduced AOD so is not driving this positive feedback in the clear-sky SW.

The dust-induced RF at TOA (−1.2 W m^{-2}) is around half the value from the ice sheet albedo alone and therefore could make a substantial contribution to the global radiation budget at the LGM, as found in some prior work. The net LGM-PI radiative forcing for the HadGEM2-A-DEAD model setup is substantially smaller, at only −0.37 W m^{-2}. In these two cases, the dust net TOA forcing is between 4% and 14% of the combined forcing from ice sheets, orography, and reduced GHG concentrations.

4. Discussion

One interesting feature of these simulations is the failure with either model to reproduce the Greenland ice core-derived increase in deposition at the LGM relative to the preindustrial. This underestimate is notable given that the potential dust source area over Asia has greatly expanded (see Figure 2). This suggests either a missing process or a low sensitivity in the dust model. Previous analyses with HadGEM2-ES have shown that it does not capture the interannual variability of dust carried across the Atlantic to Barbados [*Booth et al.*, 2012], and perhaps a lack of stronger dust storm events in Asia also (which is known to be the major source region for Greenland ice core dust [e.g., *Svensson et al.*, 2000]) is responsible for the underestimate of the LGM dust

flux at Greenland. There is also a cold bias in the model in Asia in both the preindustrial and LGM [*Hopcroft and Valdes*, 2014]. This will strongly impact on emission strengths at the LGM as subzero temperatures and snow cover both inhibit emissions in the CLASSIC, while snow cover prevents emissions in this version of the DEAD scheme. With the Spectral Radiation-Transport Model for Aerosol Species, *Takemura et al.* [2009] simulated an increase in dust deposition over 60° – 90°N by nearly 22 times at the LGM. This is driven by a significant increase in emissions over Europe and Asia. Part of this likely derives from a different formulation for dust mobilization source area which in the *Takemura et al.* [2009] model is a function of leaf area index rather than bare soil as used in HadGEM2.

In the model intercomparison of *Huneeus et al.* [2011], it was shown that integrated properties such as AOD and radiative effects vary by around a factor of 2 between models, but for dust deposition rates, the inter-model variability increases to a factor of 10. This suggests that constraining the dust cycle with estimates of deposition changes between two climates could therefore be subject to a high level of uncertainty. This result is supported here by the similarity between the dust deposition fields in two different schemes, while there is large (factor of three) difference in TOA LGM-PI dust radiative forcing.

Recent work on the size distribution of dust emissions [*Kok*, 2011] suggests that current models tend to overestimate the fraction of fine particles in emitted dust. Finer particles have stronger radiative cooling effects than the coarser particles, implying that in a model which overestimates fine-particle fraction but simulates dust loading correctly, the total AOD from dust may be in error and radiative effects may be overestimated. Conversely, if the model AOD is well matched to observations, then the total mass of dust is likely to be in error and this means that models may underestimate the quantity of dust emitted. Differences between the older versions of HadGEM2 CLASSIC and DEAD schemes in terms of the size distribution of dust near the Sahara found by *Ackerley et al.* [2012] are not as large in our simulations. However, the CLASSIC scheme is in better agreement with the clay fraction (the proportion of particles smaller than 2 μm) values proposed by *Kok* [2011].

In general, the particle size distribution as well as a variety of other factors is important for the dust radiative properties including particle shape and mixing of elemental composition [e.g., *Claquin et al.*, 2003; *Durant et al.*, 2009]. In HadGEM2, the refractive indices are taken from Saharan dust values of *Balkanski et al.* [2007] and these may not be suitable for sources further afield, for example, Australian dust, which is known to have a higher hematite content and so is more absorbing and less reflective in the SW, or additional sources unique to the LGM, for example, in Patagonia.

Inclusion of the interactions between mineral dust and clouds is missing in the model setup used here. Mineral dust is thought to be an important source of ice nuclei, but this process has not yet been included in the current or newer UK Met Office climate model versions [*Bellouin et al.*, 2013]. Previous work had suggested that the indirect aerosol effects of mineral dust are larger than the direct effects for the LGM climate [*Takemura et al.*, 2009], primarily because of an increase in the ice water cloud amount, and this mechanism for dust-cloud interaction deserves further study.

Another process that could impact on the radiative forcing and feedback analysis is the impact of dust deposition on snow and ice albedo which plays an important role in modern-day glacier mass balance [*Dumont et al.*, 2014]. This has been modeled for the Last Glacial Maximum by *Krinner et al.* [2006] who suggested that it restricted glaciation in Northern Eurasia. It may also play a role in the global climate response to dust as the total snow- or ice-covered area of the LGM was significant. Furthermore, darker snow would enhance the radiative effects from dust emitted over high-latitude regions and this could modify significantly the regional sensitivity to an enhanced dust loading.

5. Conclusions

The mineral dust cycle in two versions [CLASSIC *Bellouin et al.*, 2011; *Woodward*, 2011; and DEAD *Zender et al.*, 2003] of the CMIP5 model HadGEM2-A shows substantial changes in response to LGM climate. Overall emissions in two versions of the HadGEM2-A model are increased by factors of 1.6 and 1.9 for the CLASSIC and DEAD schemes, respectively. Simulations with fixed modern-day observed vegetation suggest that physical climate changes alone are responsible for only a small fraction of this increase. The size distribution of uplifted dust differs markedly between the two uplift schemes examined, with the DEAD scheme dominated by fine <3 μm radius particles, while in the CLASSIC scheme the mixture is dominated by >10 μm particles. However,

the strong size dependence of sedimentation in particular results in the size distributions of the atmospheric dust burden being more similar: the distribution peaks at 1–3.16 μm in both CLASSIC and DEAD models for both time periods.

The model shows most sensitivity in the Southern Hemisphere, particularly over South America where a substantial new area of bare soil emerges. This drives dust flux increase over the Southern Atlantic which is slightly larger than reconstructed from the data, but leading to depositional increases that are less than reconstructed from Antarctic ice cores. This result is consistent with the overestimate of preindustrial dust emissions from Australia in HadGEM2 [e.g., *Bellouin et al.*, 2011] which means that the LGM/PI deposition ratio over Antarctica is biased low. The DEAD scheme results show larger relative changes in deposition in the Southern Ocean and Antarctica. This is because of the different emission rates in the middle bins 3 and 4 in the two schemes and because the DEAD scheme has around three times the rate of wet deposition of the CLASSIC scheme (Table 3).

In terms of radiative forcing and aerosol optical depth, the schemes show similar patterns of change, but with much larger anomalies in the CLASSIC scheme. The CLASSIC scheme shows much higher sensitivity to glacial climate for the smaller particle divisions, explaining the larger LGM-PI SW radiative forcing in this scheme. The LGM-PI LW radiative forcing is actually comparable in the two schemes. The emitted mass from bin 4 is larger in DEAD and constitutes a larger fraction of the total emitted flux. Since much of the LW radiative forcing is driven by particles in this size bin, the LW forcing is comparable in DEAD and CLASSIC. The two models simulate a net TOA dust forcing that is between 4% and 14% of the total climate forcing at the LGM relative to the preindustrial. These figures are likely to underestimate the true dust forcing at the LGM because other sources of dust from glaciogenic sources are not included [e.g., *Mahowald et al.*, 2006a; *Sugden et al.*, 2009].

The use of a single threshold friction velocity in DEAD and other schemes [e.g., *Takemura et al.*, 2009; *Albani et al.*, 2014] is in contradiction with theory [*Iversen and White*, 1982] and may bias the simulation of radiative forcing changes between different climatic states. Here we demonstrate that the size distribution of uplifted dust is important for determining the eventual radiative effects [similar conclusions are reached by *Albani et al.*, 2014]. We also highlight the key role played by parameterization of threshold friction velocity and other aspects of the dust emissions, in determining the radiative forcing between different climatic states, a factor that has not been explored in prior work.

In our simulations, two model versions with very different radiative forcing are in fact surprisingly similar in terms of how well they compare with the reconstructed dust depositional fluxes in the present and past. This demonstrates that the total deposition flux reconstructions are inadequate for discerning between different representations of the LGM-PI dust cycle change. At least in HadGEM2, the deposition is mostly sensitive to changes in the flux of larger (2–6 μm diameter) particles, whereas the SW radiative effects which dominate the overall radiative forcing are predominantly driven by changes in the loading of finer (<2μm diameter) particles.

This implies that other measures of the dust cycle may be required in order to constrain the impacts of dust in past climates like the LGM and, secondly, that it is difficult to constrain the role of dust in terms of fertilizing ocean and terrestrial carbon cycles. *Mahowald et al.* [2014] also highlight uncertainties in dust size distribution changes as a function of depositional processes and in resolving with models the size distribution tails of very fine and very large particles. Future model evaluations should make use of newly available measurements [e.g., *McConnell et al.*, 2008; *Ryder et al.*, 2013] to better constrain the particle size makeup of modeled dust emissions and tropospheric loading. Further analysis of dust size distribution in sediments and ice core data may also provide similar information from past climate states [*Maher et al.*, 2010; *Albani et al.*, 2012, 2014] and help to improve model simulations of the past and future.

Acknowledgments

We thank Karen Kohfeld for discussions on various aspects of this work, and Nicolas Bellouin for helping us to set up the double-call radiative forcing simulations. All HadGEM2 simulations were run on the HECToR or ARCHER national facilities. P.O.H. was funded by the UK NERC project Earth System Modelling of Abrupt Climate Change (NE/I010912/1). S.W. was supported by the Joint UK DECC/Defra Met Office Hadley Centre Climate Programme (GA01101). We acknowledge the World Climate Research Programme's Working Group on Coupled Modelling, which is responsible for CMIP, and the climate modeling groups for producing and making available their model output. For CMIP the U.S. Department of Energy's Program for Climate Model Diagnosis and Intercomparison provided coordinating support and led development of software infrastructure in partnership with the Global Organization for Earth System Science Portals. All model output is available from www.bridge.bris.ac.uk/resources/simulations. Please contact P.O.H. or P.J.V. for access.

References

Ackerley, D., et al. (2009), The development of a new dust uplift scheme in the Met Office Unified Model™, *Meteorological Applications*, *16*, 445–460, doi:10.1002/met.141.

Ackerley, D., M. Joshi, E. Highwood, C. Ryder, M. Harrison, D. Walters, S. Milton, and J. Strachan (2012), A comparison of two dust uplift schemes within the same general circulation model, *Adv. Meteorol.*, *2012*, 260515, doi:10.1155/2012/260515.

Albani, S., N. Mahowald, B. Delmonte, V. Maggi, and G. Winckler (2012), Comparing modeled and observed changes in mineral dust transport and deposition to Antarctica between the Last Glacial Maximum and current climates, *Clim. Dyn.*, *38*(9–10), 1731–1755, doi:10.1007/s00382-011-1139-5.

Albani, S., N. Mahowald, A. Perry, R. Scanza, C. Zender, N. Heavens, V. Maggi, J. Kok, and B. Otto-Bleisner (2014), Improved dust representation in the community atmosphere model, *J. Adv. Model. Earth Syst.*, *6*, 541–570, doi:10.1002/2013MS000279.

Andersen, K., A. Armengaud, and C. Genthon (1998), Atmospheric dust under glacial and interglacial conditions, *Geophys. Res. Lett.*, *25*(13), 2281–2284.

Ansmann, A., et al. (2008), Influence of Saharan dust on cloud glaciation in southern Morocco during the Saharan Mineral Dust Experiment, *J. Geophys. Res.*, *113*, D04210, doi:10.1029/2007JD008785.

Bagnold, R. (1941), *The Physics of Blown Sand and Desert Dunes*, Methuen, London.

Balkanski, Y., M. Schulz, T. Claquin, and S. Guibert (2007), Reevaluation of mineral aerosol radiative forcings suggests a better agreement with satellite and AERONET data, *Atmos. Chem. Phys.*, *7*, 81–95.

Bellouin, N., O. Boucher, J. Haywood, C. Johnson, A. Jones, J. Rae, and S. Woodward (2007), Improved representation of aerosols for HadGEM2, *Hadley Cent. Tech. Note 73*, Met Office Hadley Centre, Exeter, U. K.

Bellouin, N., J. Rae, A. Jones, C. Johnson, J. Haywood, and O. Boucher (2011), Aerosol forcing in the CMIP5 simulations by HadGEM2-ES and the role of ammonium nitrate, *J. Geophys. Res.*, *116*, D20206, doi:10.1029/2011JD016074.

Bellouin, N., G. W. Mann, M. T. Woodhouse, C. Johnson, K. S. Carslaw, and M. Dalvi (2013), Impact of the modal aerosol scheme GLOMAP-mode on aerosol forcing in the Hadley Centre Global Environmental Model, *Atmos. Chem. Phys.*, *13*, 3027–3044.

Booth, B., N. Dunstone, P. Halloran, T. Andrews, and N. Bellouin (2012), Aerosols implicated as a prime driver of twentieth-century North Atlantic climate variability, *Nature*, *484*(7393), 228–232, doi:10.1038/nature10946.

Bopp, L., K. Kohfeld, and C. Le Quere (2003), Dust impact on marine biota and atmospheric CO_2 during glacial periods, *Paleoceanography*, *18*(2), 1046, doi:10.1029/2002PA000810.

Braconnot, P., et al. (2007), Results of PMIP2 coupled simulations of the Mid-Holocene and Last Glacial Maximum part 1: Experiments and large-scale features, *Clim. Past.*, *3*, 261–277.

Braconnot, P., S. Harrison, M. Kageyama, P. Bartlein, V. Masson-Delmotte, A. Abe-Ouchi, B. Otto-Bliesner, and Y. Zhao (2012), Evaluation of climate models using palaeoclimatic data, *Nat. Clim. Change*, *2*, 417–424, doi:10.1038/nclimate1456.

Bristow, C., K. Hudson-Edwards, and A. Chappell (2010), Fertilizing the Amazon and equatorial Atlantic with West African dust, *Geophys. Res. Lett.*, *37*, L14807, doi:10.1029/2010GL043486.

Chase, Z., R. Anderson, and M. Fleisher (2001), Evidence from authigenic uranium for increased productivity of the glacial subantarctic ocean, *Paleoceanography*, *16*(5), 468–478.

Claquin, T., et al. (2003), Radiative forcing of climate by ice-age atmospheric dust, *Clim. Dyn.*, *20*, 193–202.

Clark, P., A. S. Dyke, J. D. Shakun, A. E. Carlson, J. Clark, B. Wohlfarth, J. X. Mitrovica, S. W. Hostetler, and A. M. McCabe (2009), The Last Glacial Maximum, *Science*, *325*, 710–714, doi:10.1126/science.1172873.

Collins, W., et al. (2011), Development and evaluation of an Earth-system model—HadGEM2, *Geosci. Model Dev.*, *4*, 1051–1075, doi:10.5194/gmd-4-1051-2011.

Cox, P. (2001), Description of the TRIFFID dynamic global vegetation model, *Hadley Cent. Tech. Note 24*, Hadley Centre, Met Office, Bracknell, U. K.

Cox, P., R. Betts, C. Jones, S. Spall, and I. Totterdell (2000), Acceleration of global warming due to carbon-cycle feedbacks in a coupled climate model, *Nature*, *408*, 184–1887.

Delmonte, B., J. Petit, and V. Maggi (2002), Glacial to Holocene implications of the new 27000-year dust record from the EPICA Dome C (East Antarctica) ice core, *Clim. Dyn.*, *18*, 647–660, doi:10.1007/s00382-001-0193-9.

Delmonte, B., I. Basile-Doelsch, J. Petit, V. Maggi, M. Revel-Rolland, A. Michard, E. Jagoutz, and F. Grousset (2004), Comparing the Epica and Vostok dust records during the last 220,000 years: Stratigraphical correlation and provenance in glacial periods, *Earth Sci. Rev.*, *66*(1–2), 63–87, doi:10.1016/j.earscirev.2003.10.004.

Dumont, M., E. Brun, G. Picard, M. Michou, Q. Libois, J.-R. Petit, M. Geyer, S. Morin, and B. Josse (2014), Contribution of light-absorbing impurities in snow to Greenland's darkening since 2009, *Nat. Geosci.*, *7*, 509–512, doi:10.1038/ngeo2180.

Durant, A., S. Harrison, H. Watson, and Y. Balkanski (2009), Sensitivity of direct radiative forcing by mineral dust to particle characteristics, *Prog. Phys. Geog.*, *33*, 80–102, doi:10.1177/0309133309105034.

Essery, R., M. Best, R. Betts, P. Cox, and C. Taylor (2003), Explicit representation of subgrid heterogeneity in a GCM land-surface scheme, *J. Hydrometeorol.*, *4*, 530–543.

Fécan, F., B. Marticorena, and G. Bergametti (1999), Parametrization of the increase of the Aeolian erosion threshold wind friction velocity due to soil moisture for arid and semi-arid areas, *Ann. Geophys.*, *17*, 149–157.

Fischer, H., M.-L. Siggaard-Andersen, U. Ruth, R. Röthlisberger, and E. Wolff (2007), Glacial/interglacial changes in mineral dust and sea-salt records in polar ice cores: Sources, transport, and deposition, *Rev. Geophys.*, *45*, RG1002, doi:10.1029/2005RG000192.

HadGEM2 Development Team (2011), The HadGEM2 family of Met Office Unified Model climate configurations, *Geosci. Model Dev.*, *4*, 7233–757, doi:10.5194/gmd-4-723-2011.

Hargreaves, J., J. Annan, M. Yoshimori, and A. Abe-Ouchi (2012), Can the Last Glacial Maximum constrain climate sensitivity?, *Geophys. Res. Lett.*, *39*, L24702, doi:10.1029/2012GL053872.

Harrison, S., K. Kohfeld, C. Roelandt, and T. Claquin (2001), The role of dust in climate changes today, at the Last Glacial Maximum and in the future, *Earth Sci. Rev.*, *54*, 43–80.

Haywood, J., and O. Boucher (2000), Estimates of the direct and indirect radiative forcing due to tropospheric aerosols: A review, *Rev. Geophys.*, *38*(4), 513–543.

Hopcroft, P., and P. Valdes (2014), Last Glacial Maximum constraints on the Earth system model HadGEM2-ES, *Clim. Dyn.*, doi:10.1007/s00382-014-2421-0, in press.

Huneeus, N., et al. (2011), Global dust model intercomparison in AeroCom phase I, *Atmos. Chem. Phys.*, *11*, 7781–7816, doi:10.5194/acp-11-7781-2011.

Iversen, J., and B. White (1982), Saltation threshold on Earth, Mars, and Venus, *Sedimentology*, *29*, 111–119.

Jones, C., D. Roberts, M. Woodage, and C. Johnson (2001), Indirect sulphate aerosol forcing in a climate model with an interactive sulphur cycle, *J. Geophys. Res.*, *106*, 20,293–20,310.

Jones, C., et al. (2011), The HadGEM2-ES implementation of CMIP5 centennial simulations, *Geosci. Model Dev.*, *4*, 543–570.

Kohfeld, K., and S. Harrison (2001), DIRTMAP: The geological record of dust, *Earth Sci. Rev.*, *54*, 81–114.

Kohfeld, K., R. M. Graham, A. M. De Boer, L. C. Sime, E. W. Wolff, C. Le Quere, and L. Bopp (2013), Southern Hemisphere westerly wind changes during the Last Glacial Maximum: Paleo-data synthesis, *Quat. Sci. Rev.*, *68*, 76–95, doi:10.1016/j.quascirev.2013.01.017.

Kok, J. (2011), A scaling theory for the size distribution of emitted dust aerosols suggests climate models underestimate the size of the global dust cycle, *Proc. Natl. Acad. Sci. U.S.A.*, *108*(3), 1016–1021.

Koren, I., Y. Kaufman, R. Washington, M. Todd, Y. Rudich, J. V. Martins, and D. Rosenfeld (2006), The Bodélé depression: A single spot in the Sahara that provides most of the mineral dust to the Amazon forest, *Environ. Res. Lett.*, *1*, 014005, doi:10.1088/1748-9326/1/1/014005.

Krinner, G., O. Boucher, and Y. Balkanski (2006), Ice-free glacial northern Asia due to dust deposition on snow, *Clim. Dyn.*, *27*, 613–625, doi:10.1007/s00382-006-0159-z.

Lambert, F., B. Delmonte, J. R. Petit, M. Bigler, P. R. Kaufmann, M. A. Hutterli, T. F. Stocker, U. Ruth, J. P. Steffensen, and V. Maggi (2008), Dust -climate couplings over the past 800,000 years from the EPICA Dome C ice core, *Nature*, *452*(3), 616–619, doi:10.1038/nature06763.

Loveland, T., B. Reed, J. Brown, D. Ohlen, Z. Zhu, L. Yang, and J. Merchant (2000), Development of a global land cover characteristics database and IGBP DISCover from 1 km AVHRR data, *Int. J. Remote Sens.*, *21*(6–7), 1303–1330.

Lunt, D., and P. Valdes (2002), Dust deposition and provenance at the Last Glacial Maximum and present day, *Geophys. Res. Lett.*, *29*(22), 2085, doi:10.1029/2002GL015656.

Maher, B., J. Prospero, D. Mackie, D. Gaiero, P. Hess, and Y. Balkanski (2010), Global connections between aeolian dust, climate and ocean biogeochemistry at the present day and at the last glacial maximum, *Earth Sci. Rev.*, *99*, 61–97, doi:10.1016/j.earscirev.2009.12.001.

Mahowald, N., K. Kohfeld, M. Hansson, Y. Balkanski, S. P. Harrison, I. C. Prentice, M. Schulz, and H. Rodhe (1999), Dust sources and deposition during the last glacial maximum and current climate: A comparison of model results with paleodata from ice cores and marine sediments, *J. Geophys. Res.*, *104*, 15,895–15,916.

Mahowald, N., S. Albani, J. Kok, S. Engelstaeder, R. Scanza, D. Ward, and M. Flanner (2014), The size distribution of desert dust aerosols and its impact on the earth system, *Aeolian Res.*, *15*, 53–71, doi:10.1016/j.aeolia.2013.09.002.

Mahowald, N. M., D. Muhs, S. Levis, P. Rasch, M. Yoshioka, C. Zender, and C. Luo (2006a), Change in atmospheric mineral aerosols in response to climate: Last glacial period, preindustrial, modern, and doubled carbon dioxide climates, *J. Geophys. Res.*, *111*, D10202, doi:10.1029/2005JD006653.

Mahowald, N. M., M. Yoshioka, W. D. Collins, A. J. Conley, D. W. Fillmore, and D. B. Coleman (2006b), Climate response and radiative forcing from mineral aerosols during the Last Glacial Maximum, pre-industrial, current and doubled-carbon dioxide climates, *Geophys. Res. Lett.*, *33*, L20705, doi:10.1029/2006GL026126.

Marticorena, B., and G. Bergametti (1995), Modelling the atmospheric dust cycle: 1. Design of a soil-derived dust emission scheme, *J. Geophys. Res.*, *100*(D8), 16,415–16,430.

Martin, G., M. A. Ringer, V. D. Pope, A. Jones, C. Dearden, and T. J. Hinton (2006), The physical properties of the atmosphere in the new Hadley Centre Global Environmental Model (HadGEM1). Part I: Model description and global climatology, *J. Clim.*, *19*, 1274–1301.

Martin, J. (1990), Glacial-interglacial CO_2 change: The iron hypothesis, *Paleoceanography*, *5*(1), 1–13.

Martinez-Garcia, A., A. Rosell-Mele, S. L. Jaccard, W. Geibert, D. M. Sigman, and G. H. Haug (2011), Southern Ocean dust-climate coupling over the past four million years, *Nature*, *476*, 312–316, doi:10.1038/nature10310.

McConnell, C., E. J. Highwood, H. Coe, P. Formenti, B. Anderson, S. Osborne, S. Nava, K. Desboeufs, G. Chen, and M. A. J. Harrison (2008), Seasonal variations of the physical and optical characteristics of Saharan dust: Results from the Dust Outflow and Deposition to the Ocean (DODO) experiment, *J. Geophys. Res.*, *1113*, D14S05, doi:10.1029/2007JD009606.

McConnell, J., A. J. Aristarain, J. R. Banta, P. R. Edwards, and J. C. Simoes (2007), 20th-century doubling in dust archived in an antarctic peninsula ice core parallels climate change and desertification in South America, *Proc. Natl. Acad. Sci. U.S.A.*, *104*(14), 5743–5748, doi:10.1073/pnas.0607657104.

Peltier, W. (2004), Global glacial isostasy and the surface of the ice age earth: The ICE-5G (VM2) model and GRACE, *Annu. Rev. Earth Planet. Sci.*, *32*, 111–149.

Petit, J., et al. (1999), Climate and atmospheric history of the past 420,000 years from the Vostok Ice Core, Antarctica, *Nature*, *399*, 429–436.

Prospero, J., and P. Lamb (2003), African droughts and dust transport to the Caribbean: Climate change implications, *Science*, *302*, 1024–1027.

Raiswell, R., L. G. Benning, M. Tranter, and S. Tulaczyk (2007), Bioavailable iron in the Southern Ocean: The significant of the iceberg conveyor belt, *Geochem. Trans.*, *9*, 7, doi:10.1186/1467-4866-9-7.

Ryder, C., et al. (2013), Optical properties of Saharan dust aerosol and contribution from the coarse mode as measured during the Fennec 2011 aircraft campaign, *Atmos. Chem. Phys.*, *13*, 303–325, doi:10.5194/acp-13-303-2013.

Sassen, K., P. J. DeMott, J. M. Prospero, and M. R. Poellot (2003), Saharan dust storms and indirect aerosol effects on clouds: CRYSTAL-FACE results, *Geophys. Res. Lett.*, *30*(12), 1633, doi:10.1029/2003GL017371.

Schneider von Deimling, T., A. Ganopolski, H. Held, and S. Rahmstorf (2006), How cold was the last glacial maximum?, *Geophys Res Lett*, *33*, L14709, doi:10.1029/2006GL026484.

Singarayer, J., and P. Valdes (2010), High-latitude climate sensitivity to ice-sheet forcing over the last 120 kyr, *Quat. Sci. Rev.*, *29*(1–2), 43–55, doi:10.1016/j.quascirev.2009.10.011.

Soden, B., A. Broccoli, and R. Hemler (2004), On the use of cloud forcing to estimate cloud feedback, *J. Clim.*, *17*, 3661–3665.

Steffensen, J. (1997), The size distribution of microparticles from selected segments of the greenland ice core project ice core representing different climatic periods, *J. Geophys. Res.*, *102*(C12), 26,755–26,763.

Sugden, D., R. D. McCulloch, A. J.-M. Bory, and A. S. Hein (2009), Influence of Patagonian glaciers on Antarctic dust deposition during the last glacial period, *Nat. Geosci.*, *2*, 281–285, doi:10.1038/NGEO474.

Svensson, A., P. Biscaye, and F. Grousset (2000), Characterization of late glacial continental dust in the Greenland Ice Core Project ice core, *J. Geophys. Res.*, *105*(D4), 4637–4656.

Takemura, T., M. Egashira, K. Matsuzawa, H. Ichijo, R. O'ishi, and A. Abe-Ouchi (2009), A simulation of the global distribution and radiative forcing of soil dust aerosols at the Last Glacial Maximum, *Atmos. Chem. Phys.*, *9*(20), 3061–3073, doi:10.5194/acp-9-3061-2009.

Taylor, K., M. Crucifix, P. Braconnot, C. Hewitt, C. Doutriaux, A. Broccoli, J. Mitchell, and M. Webb (2007), Estimating shortwave radiative forcing and response in climate models, *J Clim.*, *20*, 2530–2543.

Tegen, I., A. Lacis, and I. Fung (1996), The influence on climate forcing of mineral aerosols from disturbed soils, *Nature*, *380*, 419–422.

Werner, M., I. Tegen, S. Harrison, K. Kohfeld, I. Prentice, Y. Balkanski, H. Rodhe, and C. Roelandt (2002), Seasonal and interannual variability of the mineral dust cycle under present and glacial climate conditions, *J. Geophys. Res.*, *107*(D24), 4744, doi:10.1029.2002JD002365.

Wolff, E. W., J. Chappellaz, T. Blunier, S. O. Rasmussen, and A. Svensson (2010), Millennial-scale variability during the last glacial: The ice core record, *Quat. Sci. Rev.*, *29*(21–22), 2828–2838, doi:10.1016/j.quascirev.2009.10.013.

Woodward, S. (2001), Modeling the atmospheric life cycle and radiative impact of mineral dust in the Hadley Centre climate model, *J. Geophys. Res.*, *106*(D16), 18,155–18,166.

Woodward, S. (2011), Mineral dust in HadGEM2, *Hadley Centre Tech. Note 87*, Met Office Hadley Cent., Exeter, U. K.

Wu, G., T. Yao, B. Xu, L. Tian, C. Zhang, and X. Zhang (2009), Volume-size distribution of microparticles in ice cores from the Tibetan plateau, *J. Glaciol.*, *55*(193), 859–868.

Yoshimori, M., T. Yokohata, and A. Abe-Ouchi (2009), A comparison of climate feedback strength between CO2 doubling and LGM experiments, *J. Clim.*, *22*, 3374–3395.

Yoshioka, M., et al. (2007), Impact of desert dust radiative forcing on Sahel precipitation: Relative importance of dust compared to sea surface temperature variations, vegetation changes, and greenhouse gas warming, *J. Clim.*, *20*, 1445–1467, doi:10.1175/JCLI4056.1.

Yue, X., H. Wang, H. Liao, and D. Jiang (2011), Simulation of the direct radiative effect of mineral dust aerosol on the climate at the Last Glacial Maximum, *J. Clim.*, *24*, 843–858, doi:10.1175/2010JCLI3827.1.

Zender, C., H. Bian, and D. Newman (2003), Mineral Dust Entrainment and Deposition (DEAD) model: Description and 1990s dust climatology, *J. Geophys. Res.*, *108*(D14), 4416, doi:10.1029/2002JD002775.